THE EFFECT OF SOURCE IMPEDANCE ON DAMPING MEASUREMENTS USING RESONANCE DWELL TESTING

by
Ralph E. Tate
LTV Aircraft Products Group
Dallas, Texas

ABSTRACT

J.C. Heine developed a test methodology for evaluating the damping in various materials, particularly metals. LTV employs a resonance dwell technique adapted from that of J.C. Heine, which facilitates the use of a smaller shaker from that normally required. This test apparatus permits the rapid characterization of viscoelastic laminates not only for damping, but also for vibroacoustical fatigue resistence.

During check-out of the modified apparatus, it was found that the behavior of damped specimens differed markedly from prior results. That is, significantly higher values of damping were observed regardless of measurement technique. The author demonstrates, through the use of impedance modeling techniques, that the differences arise from the coupling the specimen to the electrodynamics of the excitation source. A refinement of the test procedure is outlined to remedy the data anomaly and a discussion of the impact on the interpretation of damping data naturally follows.

1.0 INTRODUCTION

Various techniques are employed throughout industry to evaluate the complex modulus of viscoelastic materials. Perhaps, the most common techniques are the "Oberst" beam-type tests that are prescribed in the ASTM standards [1]. The simplicity of the test method affords rapid evaluation of a candidate viscoelastic with a minimal investment in material and equipment.

The cited standard, ASTM E756-83 [1], provides three alternative cantilever beam test specimen configurations, depending on whether shear or tensile modulus is to be measured. The standard presumes base motion acceleration excitation. The standard also provides a set of equations to compute the viscoelastic's material loss factor from the specimen's sample loss factor, based on the Ross-Kerwin-Ungar (RKU) equations for damped laminates.

LTV employs a resonance dwell methodology adapted from that of JC Heine [2], which facilitates the use of a smaller shaker. The test apparatus is depicted in Figure 1. This particular testing apparatus permits evaluation of viscoelastic laminates not only for damping properties, but for vibro-acoustical fatigue resistance, as well. This paper describes the analytical mechanics of this method of resonance dwell testing of constrained layer laminates, based on a motivating example arising from adaption of the test apparatus to perform fatigue testing. Further, comparisons of test results from resonance dwell testing to published nomogram data for viscoelastic materials are discussed .

2.0 "HEINE'S" METHOD

JC Heine developed a test methodology for evaluating the damping in various materials, particularly metals (cf. Figure 1)[2]. A test beam is clamped into the root lever arm. Then, a constant shaker force is applied to the lever near the root of the beam. The shaker force is varied until the tip deflection peaks and the root acceleration simultaneously minimizes. At that frequency, the test beam is said to be at resonance.

The prescription works due to the high stiffness of the lever relative to that of the test specimen. Effectively, the system is rendered mechanically uncoupled; that is, the test beam resonance is identical with that obtained from a cantilever beam under base motion excitation. Given the resonance frequency and tip deflection, the modulus and loss factor for a given material are easily estimated. For a damped constrained layer laminate, the sample loss factor is given by

$$\eta_s = \left(\frac{\phi_n a_R}{\pi^2 V_t f_d^{\,2}}\right) \frac{(\sigma_n/\lambda_n)}{[1-f_0/f_d]} \left(1+\frac{L_B}{\sigma_n \lambda_n L_R}\right),$$

and the dynamical shear modulus is given by,

$$G = 4\pi^2 f_d^{\,2} \left[1 - (f_0/f_d)^2\right]$$

$$\times \left(\frac{m_B t_3 L_B^2}{W \sigma_n \lambda_n (2+\sigma_n \lambda_n) d^2} \right).$$

(variables defined at end of paper)

3.0 TEST RESULTS

Although Heine developed his apparatus to study lightly damped materials such as metals, it is just as applicable to the testing of highly damped laminates. Further, after reduction of the lever arm stiffness, the apparatus can be effectively used to evaluate the vibroacoustical fatigue resistance of damped laminates. It then differs from many similar devices in that it provides levels of stress that are experienced by aircraft structures, while using a smaller and less expensive shaker. It was found that the behavior of the modified apparatus during tests of highly damped specimens differs markedly from its behavior during tests of lightly damped test specimens.

Some typical results of a damped constrained layer test specimen in the adapted Heine test apparatus are depicted in Figure 2. The tip deflection curve in Figure 2 was generated using the procedure developed by Heine. The transfer function shown in that figure was computed between the root acceleration and the tip deflection, as a check on the procedure. The tip deflection indicates a broader damping than the transfer function, based on standard half-power estimates [3]. Further, the tip deflection shows a lower peak frequency, and the acceleration minimized with the transfer function. Since these peculiarities of the transfer function and the base acceleration had not been observed during previous testing of lightly damped specimens, interpretation of the data became ambiguous.

A strain gage was affixed to the root of the test beam, and the test repeated. Figure 3 shows that the tip deflection and the root strain track together. Then a controller was added to maintain a constant root acceleration. Figure 4 shows that the tip deflection (as well as the root strain, not depicted) and the transfer function agree in damping and frequency, when the base acceleration is controlled. This behavior conflicts with the procedure defined by Heine.

Several indications of maximum response for damped test specimens are displayed in Figure 2 through 4. How, then, should the resonant frequency be identified, and how should the damping of the specimen be determined, once the resonant frequency is identified? The mathematical analyses described below were undertaken to answer those questions.

4.0 EQUATIONS OF MOTION

The equations of motion for the resonance dwell apparatus were developed using a standard energy method approach [4,5,6]. The analytical model used the geometry described in Figure 5. That test specimen is a laminate encompassing a constrained layer of viscoelastic damping material, as shown in Figure 6. The assumed deflection of the system is (tensor summation assumed over free subscript indices, 1 to N):

$$v(x,t) = x\,\alpha(t)\,\underline{H}(x) + \phi_i(x-\underline{L}_R)\,v_i(t)\,\underline{H}(x-L_R).$$

The virtual work due to bending of the face sheets, as shown in Figure 6, can be computed as:

$$\delta W_B = \int_{L_R}^{(L_R+L_B)} [(EI)_1+(EI)_2]\, v''\delta v''\, dx,$$

$$= [(EI)_1+(EI)_2]\,\underline{X}_{4,i}\, v_i\, \delta v_j,$$

where

$$\underline{X}_{4,i} = \begin{cases} (\beta_i)^4\, L_B, & (i=j) \\ 0, & (i\neq j, \text{ orthogonality}). \end{cases}$$

Analogously, the virtual work from lever flexure is:

$$\delta W_R = K_R\,\alpha(t)\,\delta\alpha(t).$$

Assuming plane sections of the laminated test specimen remain plane, and given that G* is the complex shear modulus of the constrained damping material shown in Figure 6, the virtual work due to shearing is [4,7]:

$$\delta W_s = \int_{L_R}^{(L_R+L_B)} t_3 G^*\,\gamma(x,t)\,\delta\gamma(x,t)\,dx,$$

$$= d^2\,(G^*/t_3)\,\underline{X}_{i,j}\, v_i\, \delta v_j, \text{ where}$$

$\underline{X}_{i,j}$ is defined as,

$$\begin{cases} \sigma_i\beta_i\,(2+\sigma_i\beta_i\,L_B) & (i=j) \\ \left(\dfrac{4\beta_i\beta_j}{\beta_i^4-\beta_j^4}\right)[(-1)^{i+j}(\sigma_j\beta_i^3-\sigma_i\beta_j^3) & \\ \quad -\beta_i\beta_j(\sigma_i\beta_i-\sigma_j\beta_j)], & (i=j). \end{cases}$$

The virtual work performed by the inertial forces can be similarly obtained. The virtual work due to acceleration of the lever arm is:

$$\delta W_L = -[J_R+M_R(L_R/2)^2]\,\ddot{\alpha}(t)\delta\alpha(t)$$
$$= -I_R\,\ddot{\alpha}(t)\,\delta\alpha(t).$$

The virtual work due to beam acceleration is ($\mu=[\rho_1 t_1+\rho_2 t_2+\rho_3 t_3]$):

$$\delta W_{B2} = -\mu \int_{L_R}^{(L_R+L_B)} \ddot{v}(x,t)\,\delta v(x,t)\,dx$$

$$= -\mu\,[\underline{X}_1\,\ddot{\alpha}\,\delta\alpha + \ddot{\alpha}\,\underline{X}_{2,i}\,\delta v_i + \delta\alpha(\underline{X}_{2,i}\,\ddot{v}_i) + \underline{X}_{3,i}\,\ddot{v}_i\,\delta v_i],$$

where

$$\underline{X}_1 = \left[\frac{(L_R+L_B)^3 - L_R}{3}\right],$$

$$\underline{X}_{2,i} = \left[\frac{2L_R\sigma_i}{\beta_i} + \frac{2}{\beta_i^2}\right],$$

and $\underline{X}_{3,i} = L_B$.

Employing the identical prescription, the virtual work performed by the applied forces becomes, including base motion:

$$\delta W_{nc1} = F L_R \delta\alpha,$$

$$\delta W_{nc2} = \frac{-M_R a_B L_R}{4} \delta\alpha, \text{ and}$$

$$\delta W_{nc3} = \mu a_B [\underline{F}_1 \delta\alpha + \underline{F}_{2,i} \delta v_i].$$

The integrals $\underline{F}_1$ and $\underline{F}_{2,i}$ are defined as follows:

$$\underline{F}_1 = \left[\frac{(L_R+L_B)^2 - L_R^2}{2}\right] - \left[\frac{(L_R+L_B)^3 - L_R^3}{L_R}\right],$$

and

$$\underline{F}_{2,i} = \frac{2\sigma_i}{\beta_i} - \frac{1}{L_R}\left(\frac{2L_B\sigma_i}{\beta_i} + \frac{2}{\beta_i^2}\right).$$

The equations of motion then can be written as:

$$\delta W_B + \delta W_R + \delta W_S - (\delta W_L + \delta W_{B2})$$

$$- (\delta W_{nc1} + \delta W_{nc2} + \delta W_{nc3}) = 0.$$

The assembled matrix form of the equations of motion is:

$$[M]\,\ddot{\underline{x}} + [K]\,\underline{x} = \underline{F}.$$

The explicit form of the matrices are given in the Appendix.

The topological features are more readily observed in matrix form. The coupling between the beam generalized coordinates is the interesting feature to be observed. The mass matrix is only coupled between each degree of freedom and the lever rotation coordinate. No inertial coupling exists between the generalized coordinates themselves.

The opposite situation is true of the stiffness matrix. The beam generalized coordinates are completely coupled through the shear compliance. Thus, for a highly damped core material, no simple closed form solution can

be obtained [8]. No stiffness coupling exists between the beam coordinates and the lever rotation.

5.0 COUPLED MODE SOLUTION

Figure 7 shows the result of a digital simulation performed incorporating the first two beam generalized coordinates and the lever rotation coordinate. The difference between the peak frequencies of the transfer function and that of the tip deflection in Figure 7 is attributable to inertial coupling of the beam with the lever arm. The coupling of both inertial and elastic structural subcomponents is a well documented phenomenon in structural mechanics [6,9,10].

The rotational stiffness of the lever was lowered to permit testing at higher strain levels approximating service fatigue environments. However, that modification lowered the lever arm resonance to near 100 Hz; that is, in the middle of the desired frequency range for testing (20 Hz to 300 Hz). Thus, the maximum tip deflection occurs at the coupled system resonance, not at the uncoupled specimen resonance. For that reason, the root strain maximizes at the coupled mode resonance, since it is there that the system is at resonance (cf. Figure 3).

The transfer function peaks at the specimen resonant frequency, since that is the relationship from root-to-tip; that is, it reflects the beam properties, per se (Figure 2). The root acceleration minimizes at the uncoupled beam frequency, since at that frequency the system observes the beam as a damper. When the root acceleration is controlled as a constant, the tip deflection and the transfer function indicate the same resonant frequency. That control enforces a base motion excitation, that effectively isolates the beam from the fixture (cf. Figure 4).

The mechanical coupling of the test specimen with the test fixture will cause an error in damping estimates, if Heine's procedure is strictly followed. First, if the frequency of maximum tip deflection is used, the damping estimate will be high, since the estimate is inversely proportional to the frequency squared [2]. Secondly, if the frequency of the minimum of the root acceleration is used, the damping estimate will again be high, since that estimate is inversely proportional to the displacement [2]. Depending on the proximity of the lever resonance to that of the test beam, a considerable error can be realized. The essential point to be considered here is: the test beam must be isolated from the fixture dynamics to obtain reliable damping estimates.

6.0 IMPEDANCE MODEL

Whereas the coupled mode solution partially described the measured frequency behavior data, the simulation did not reflect the measured damping behavior. After repeated attempts to match the difference in damping behavior between the transfer function and the tip deflection, an equivalent circuit impedance model was constructed, using a force-voltage technique (Figure 8) [11,12]. The model retained two degrees of freedom: the first beam generalized coordinate, and the lever rotation coordinate. That model maintained the important relationships between the fixture and the test beam.

The motivation for using an impedance model was the observed influence of source impedance on the electrical duals of mechancal circuits [13,14].

Summing the impedances about each loop (cf. Figure 8) and solving for the transfer impedances:

$$\frac{I_2}{V_s} = \frac{1}{A + B + j\,C}, \text{ and}$$

$$\frac{I_1}{I_2} = \frac{-j\omega M_{12}}{R_1 + jX_1}, \text{ where}$$

$$A = (R_s + R_2),$$

$$B = \frac{\omega^2 M_{12}^2 R_1}{R_1^2 + X_1^2},$$

$$C = j\left(X_2 - \frac{\omega^2 M_{12}^2 X_1}{R_1^2 + X_1^2}\right),$$

with reactances defined as,

$$X_1 = \omega L_1 - \frac{1}{\omega C_1} \text{ and } X_2 = \omega L_2 - \frac{1}{\omega C_2}.$$

Here, the dependence of the root-to-tip transfer impedance solely on the specimen properties is readily observed. Thus, the system is at resonance when the tip deflection is maximized, but the transfer impedance (or function) possesses the specimen damping property information (cf. Figure 2) [13].

Since the load should appear as a large resistance relative to the fixture, the Thevenin resistance (R_s) was tuned to nearly 50% percent of the lever arm stiffness. At that level, the analytical simulation converged to that of experiment (Figure 9). The loss factor computed from the transfer function is 0.02 and 0.045 from the tip deflection. Thus, the principal difference between the damping estimates arises from the shaker source impedance inertially coupled to the specimen through the lever arm, that is the back-EMF induces damping [19]!!

6.0 VARIANCES WITH RKU DAMPING ESTIMATES

The Ross-Kerwin-Ungar equations (RKU) were developed to evaluate the response of damped and sandwich beams [15,16] to acoustical excitation. The loss factors measured in the above analytical and measured data are somewhat lower than that expected from RKU estimates and published nomograms for viscoelastic materials. Much of the available nomogram data was developed using the RKU formulations, since those nomograms are for materials that were developed for noise and vibration control, not for sonic fatigue suppression. Based on those nomograms, loss factors at or above 0.1 should be anticipated.

The principal source of disagreement arises from the mode in which the specimen is tested.

The RKU equations assume simply supported boundary conditions[15,16]. Figure 10 shows that the eigenvalues for cantilevered beams converge to within 80% of those of simply supported beams after the third mode. (For instance, Anatrol formulates their nomograms based on the average loss factor measured from the third through sixth modes [17].) Therefore, the loss factors measured from the first or second mode will be as much as one order of magnitude lower than those found in the nomograms, since the shearing strain is concentrated at the root of the beam in those modes. That is, for the higher modes of vibration, the material is being more uniformly worked along the beam length; whereas, the lower modes of vibration only work the material near the root of the beam. This fact illustrates why constrained layer systems are effective on the higher modes, since more wavelengths are shearing the core material.

7.0 SUMMARY/CONCLUSIONS

The mechanics of a widely used resonance dwell test apparatus were developed through an energy method application, with respect to the testing methodology established by Heine using ASTM "Oberst" specimens [1,2]. Test considerations for fixturing and comparison with published data were highlighted through analysis of a practical example. The essential points to be considered are several-fold.

Firstly, the mechanics of an apparently simple apparatus can be quite complex. Failure to comprehend those subtleties can result in the acquisition of irrelevant data, especially when the test apparatus is modified from its original intent. The test procedure and ultimate application of the test data must be wholly consistent with the physical parameters of the test apparatus.

Secondly, the test specimen must be either mechanically or artifically isolated from the fixture dynamics to obtain reliable damping estimates. That is, the fixture must not possess resonances that may couple to the test specimen, or the use of a controller may be required to isolate the specimen artificially. Otherwise, the coupling must be indirectly eliminated in the data reduction, which may be unsatisfying.

Thirdly, the source and test methodology employed to develop any published nomogram data must be consistent with the particular test objectives when comparing measured test data. Lastly, although not a consideration in the above application, the effect of the root restraint should be examined, since the damped boundary condition is very difficult to effect.

Resonance dwell testing is a cost effective method of screening candidate damping materials for noise and vibration control, and sonic fatigue resistance. However, a particular methodology or apparatus cannot be used adhoc. A short reflection on the desired results and test objectives reaps a great reward in acquiring good, relevant, and inexpensive test data.

NOMENCLATURE

L_R = lever length
L_B = beam specimen length
M_R, J_R = lever inertias
W = specimen width
t_1, t_2 = facesheet thicknesses
t_3 = viscoelastic thickness
V_t = specimen tip deflection
a_R = root acceleration
a_B = base acceleration
f_B = bare specimen frequency
f_0 = damped specimen frequency
$d = t_3 + (t_1+t_2)/2$
m_B = lineal mass density
G_B = storage modulus
η_s = loss factor
$G^* = G(1+j\eta_s)$
E = facesheet elastic modulus
$v(x,t)$ = beam displacement
$\alpha(t)$ = lever rotation
$v_i(t)$ = generalized beam deflection
$\phi(x-L_R)$ = mode shape
$\underline{H}(.)$ = step function
σ_n = mode shape parameter
λ^n = eigenvalue
$\beta^n = \lambda_n / L_B$
μ^n = area mass density
F = applied shaker force
ω = angular frequency

REFERENCES

1. Anon. (1983); "Measuring Vibration-Damping Properties of Materials, Standard Method for-", ASTM STD-E756-83.

2. JC Heine(1966); "The Stress and Frequency Dependence of Material Damping Factors for Some Engineering Materials", ScD Dissertation, MIT, Cambridge, MA.

3. RW Clough and J Penzien(1975); **Dynamics of Structures**, McGraw- Hill, NY.

4. RD Blevins(1979); **Formulas for Frequency and Mode Shape**, Van Nostrand Rheinhold, NY.

5. HL Langhaar(1962); **Energy Methodsin Applied Mechanics**, John Wiley, NY.

6. RR Craig (1981); **Structural Dynamics: An Introduction to Computer Methods**, John Wiley, NY.

7. SP Timoshenko and JM Gere (1972); **Mechanics of Materials**, Van Nosstrand Rheinhold, NY.

8. JC Slater and NH Frank (1947); **Mechanics**, McGraw-Hill, NY.

9. L Meirovitch (1975); **Elements of Vibration Analysis**, McGraw-Hill, NY.

10. JS Przemieniecki (1968); **Theory of Matrix Structural Analysis**, McGraw-Hill, NY.

11. LL Beranek (1955); **Acoustics**, McGraw-Hill, NY.

12. VH Neubert (1987); **Mechanical Impedance: Modelling/Analysis of Structures**, Naval Sea Systems Command, Code NSEA-55N, DC.

13. G Koehler (1955); **Circuits and Networks**, MacMillan, NY.

14. SE Schwarz and WG Oldham (1984); **Electrical Engineering: An Introduction**, Harper Rheinhardt and Winston, NY.

15. AD Nashif, et.al. (1985); **Vibration Damping**, John Wiley, NY.

16. L Cremer, Heckl, and EE Ungar (1987); **Structure-Borne Sound**, 2nd Ed., Springer-Verlag.

17. Personal communication between ML Parin (Anatrol Corporation) and RE Tate (LTV Aircraft Products Group).

18. FF Rudder and HE Plumblee (1975); "Sonic Fatigue Design Guide for Military Aircraft", AFWAL AFFDL-TR-74-112.

19. EL Peterson, WM Rusen, and TA Mouch ; "Modal Excitation - Force Drop-Off at Resonances", **Sound and Vibration**, April 1990.

APPENDIX

The inertia matrix, stiffness matrix, and force vector were developed by application of energy methods above. The coupled inertia matrix is:

$$\begin{bmatrix} \mu\underline{X}_{3,1} & 0 & 0 & 0 & \dots & 0 & \mu\underline{X}_{2,1} \\ 0 & \mu\underline{X}_{3,2} & 0 & 0 & \dots & 0 & \mu\underline{X}_{2,2} \\ 0 & 0 & \mu\underline{X}_{3,3} & 0 & \dots & 0 & \mu\underline{X}_{2,3} \\ & & \cdot \quad \cdot & \cdot & & & \\ \mu\underline{X}_{2,1} & \mu\underline{X}_{2,2} & \mu\underline{X}_{2,3} & \dots & & \mu\underline{X}_{2,N} & \mu\underline{X}_{1} + I_R \end{bmatrix},$$

Analogously, the coupled stiffness matrix is:

$$\begin{bmatrix} (EI)\beta_1^4 + G^*X_{1,1} & G^*X_{1,2}^{} & \dots & G^*X_{1,3} & \dots G^*X_{1,N} & 0 \\ G^*X_{1,2} & (EI)\beta_2^4 + G^*X_{2,2} & & G^*X_{2,3} & \dots G^*X_{2,N} & 0 \\ & \cdot \quad \cdot & \cdot & & & \\ G^*X_{1,N} & G^*X_{2,N} & \dots & (EI)\beta_N^4 + G^*X_{N,N} & 0 & \\ 0 & 0 & & 0 & & K_R \end{bmatrix},$$

Finally, the force vector is:

$$\begin{pmatrix} \underline{F}_{2,1} \\ \underline{F}_{2,2} \\ \underline{F}_{2,3} \\ \dots \\ \underline{F}_{2,N} \\ \mu\, a_B\, \underline{F}_1 - \dfrac{M_R\, a_B\, L_R}{4} + F\, L_R \end{pmatrix},$$

where $G^* = \dfrac{G^*}{t_3}\left[t_3 + \left(\dfrac{t_1 + t_2}{2}\right)\right]^2$,

and $EI = [(EI)_1 + (EI)_2]$.

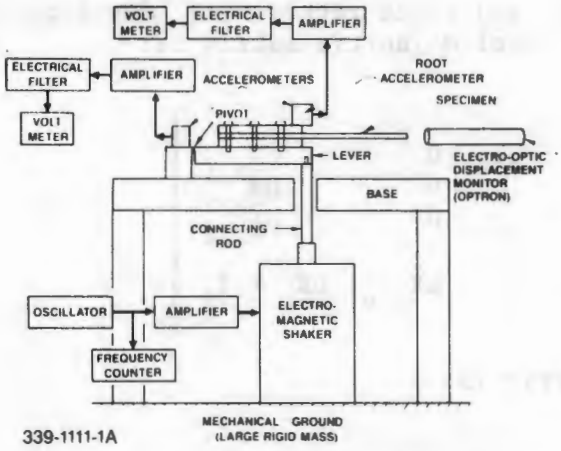

Figure 1 LTV's Resonance Dwell Apparatus

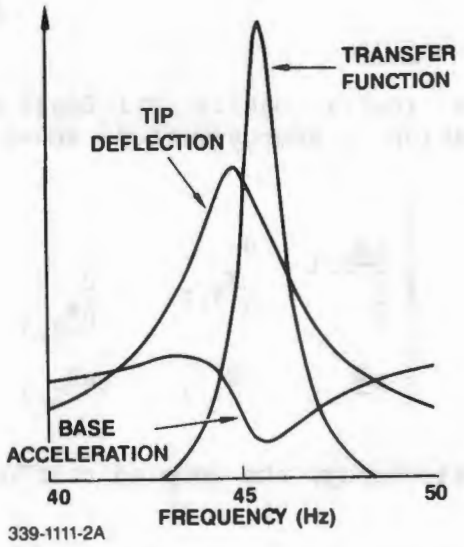

Figure 2 Response of Beam Specimen Depicting Discrepancies Versus Heine Method

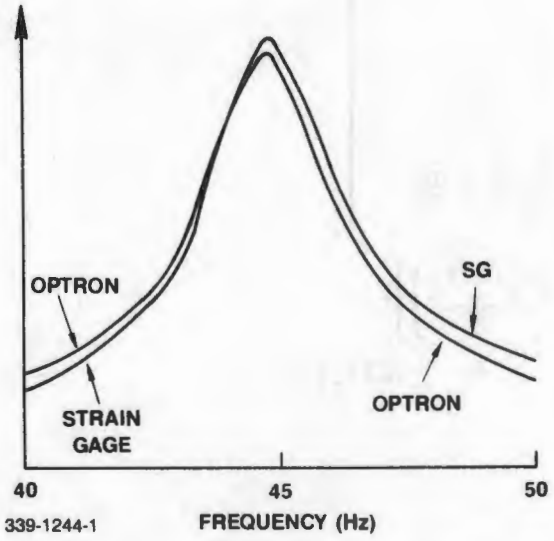

Figure 3 Tip Deflection and Root Strain - Shaker Force Constant

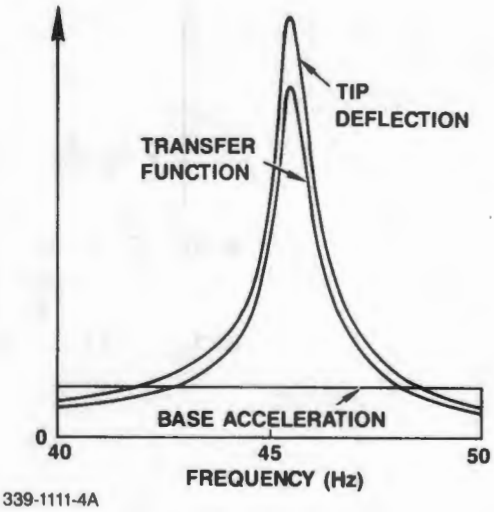

Figure 4 Tip Deflection Versus Transfer Function - Base Acceleration Constant

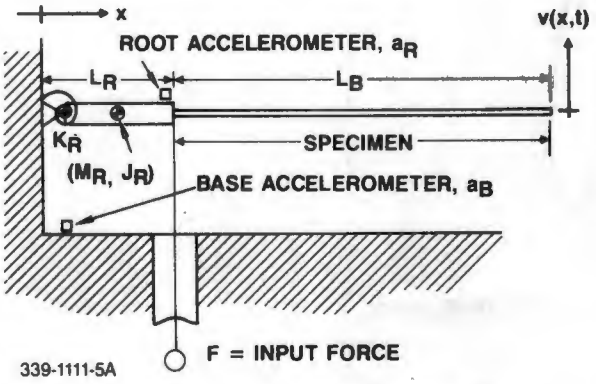

Figure 5 Analytical Geometry of the Resonance Dwell Apparatus; After Heine

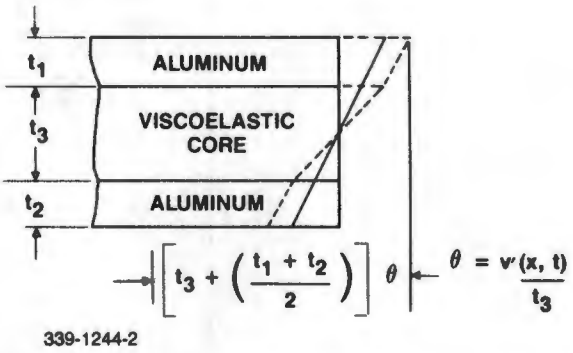

Figure 6 Geometry of Constrained Shear Layer

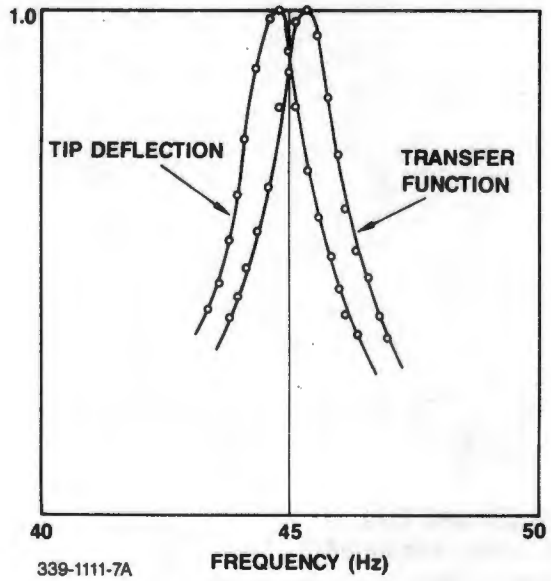

Figure 7 Coupled Response of Beam Test Specimen; Tip Deflection and Transfer Function

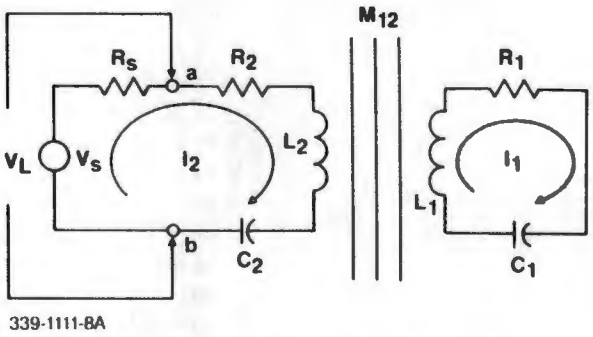

Figure 8 Equivalent Circuit for Lever Rotation (I_2) and Beam-First Mode Deflection (I_1)

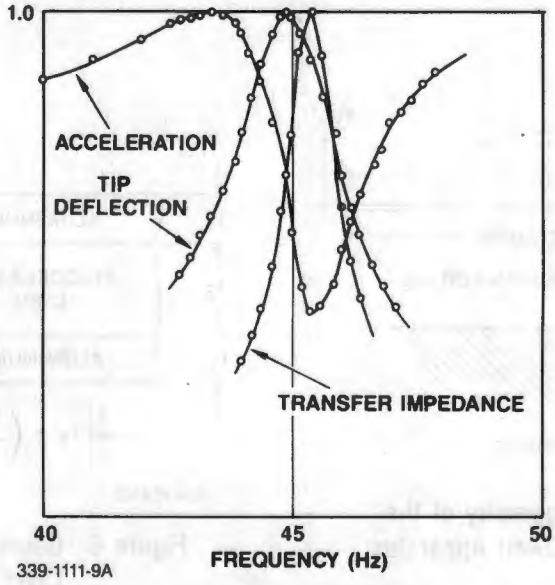

Figure 9 Normalized Acceleration and Transfer Function Depicting Convergence with Test Results

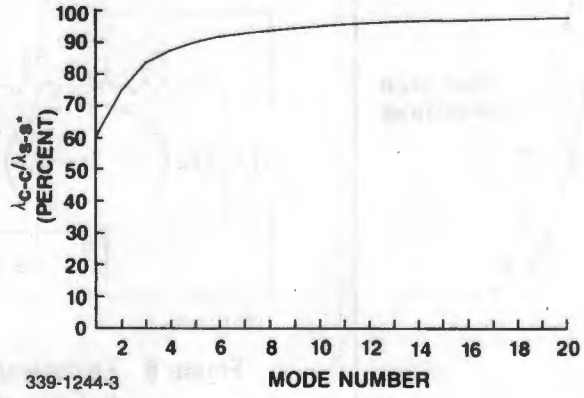

Figure 10 Convergence of Clamped-Free Eigenvalues to Simply-Supported Eigenvalues Versus Mode Number